The Design, Build, and Test of an Airfoil: An Experimental and Numerical Study on Flow Characteristics

Dylan DiGiovanni*, Jordan O'Hearn*, Roy Visser, Sanjivan Manoharan*****
School of Engineering
Grand Valley State University
Grand Rapids, MI 49504
Email: digiovad@mail.gvsu.edu, ohearnj@mail.gvsu.edu, visserro@gvsu.edu, manohars@gvsu.edu

Abstract

The flow over a custom built NACA 4414 airfoil has been investigated experimentally and numerically. This study was conducted in order to gain a deeper appreciation of flow over an external body and in the process also be exposed to certain design challenges. The numerical portion of this study consisted of determining the lift coefficient at various angles of attack for the NACA 4414 airfoil, observing the stalling point by capturing the boundary layer behavior using a fine mesh near the airfoil surface, and testing various vortex generator configurations to delay the separation of boundary layer thereby improving lift characteristics. The experimental portion involved designing and manufacturing the custom NACA 4414 airfoil in-house using 3D printing methods and testing the wing in a wind tunnel to study the selected vortex generator configuration. Mounting of the pressure taps on the airfoil surface was very challenging since the airfoil chord was only 100 mm. The project provided an opportunity to test theory by incorporating CFD and experimental techniques while overcoming various design challenges.

Introduction

The flow over an airfoil has been widely used as a classic example in fluid mechanics when talking about boundary layer separation. The boundary layer is a region of the fluid near the body where a velocity gradient exists; the fluid velocity immediately adjacent to the body is zero (no-slip) while that some distance away has the freestream value (see Fig. 1). Boundary layer separation is a phenomenon that occurs when the fluid layer adjacent to the airfoil can no longer adhere to the contour of the body and ends up lifting up and away from it.

* Undergraduate Student
** Lab Supervisor
*** Assistant Professor, Mechanical Engineering

Proceedings of the 2018 ASEE North Central Section Conference

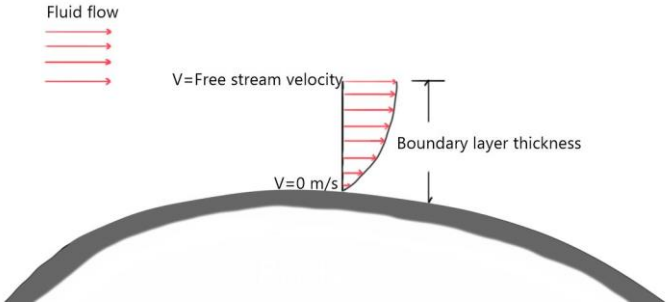

Figure 1: Boundary layer thickness illustration

As the fluid approaches the airfoil, it speeds up and at a certain point reaches maximum velocity. This point will also have the lowest pressure and until now the fluid sees a favorable (negative) pressure gradient. Beyond this point, the fluid begins to slow down and will have to fight an adverse (positive) pressure gradient before it can leave the airfoil and return to its original pressure. The layer immediate to the airfoil will witness the greatest reduction in momentum due to viscous forces. If this fluid layer does not have enough kinetic energy to negotiate this adverse pressure gradient (energy is lost due to viscous forces), it will reverse direction[1-3]. This reversed stream will then collide with the oncoming stream causing the streamlines to separate and generate vortices. At the separation point, the shear stress becomes zero.

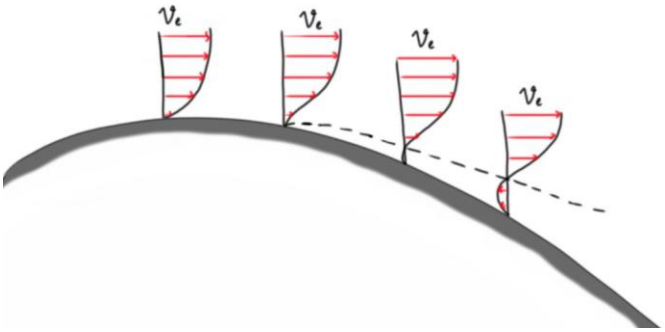

Figure 2: Boundary layer velocity distribution

The colliding streamlines create a wake (Fig. 3) which is highly undesirable since pressure drag increases significantly. The result is an increase in drag coefficient and a decrease in lift coefficient. At this point, the airfoil is said to have undergone stalling. The angle of attack at which this happens is known as the critical angle of attack. Figure 4 shows the variation of lift coefficient with angle of attack for a Clark-Y airfoil. These results were obtained from experiments conducted in-house. The critical angle of attack is around 12 deg.; this value can change depending on the airfoil characteristics considered and other various parameters.

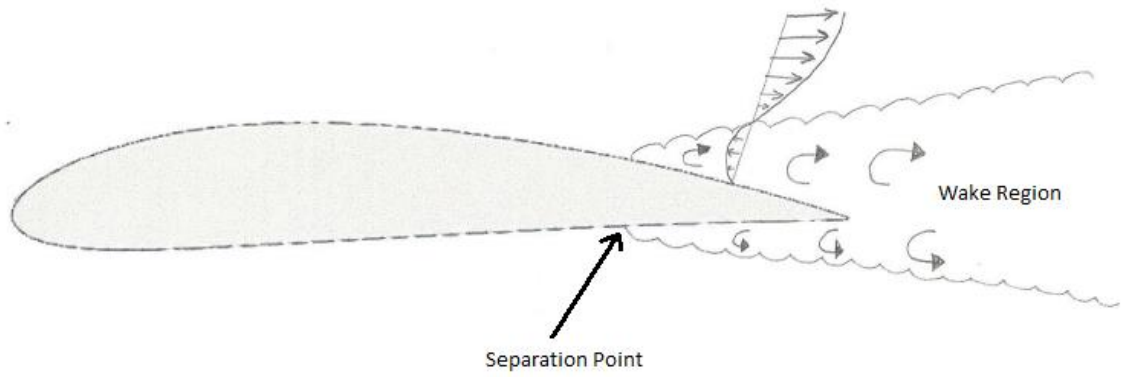

Figure 3: Sketch showing the wake region

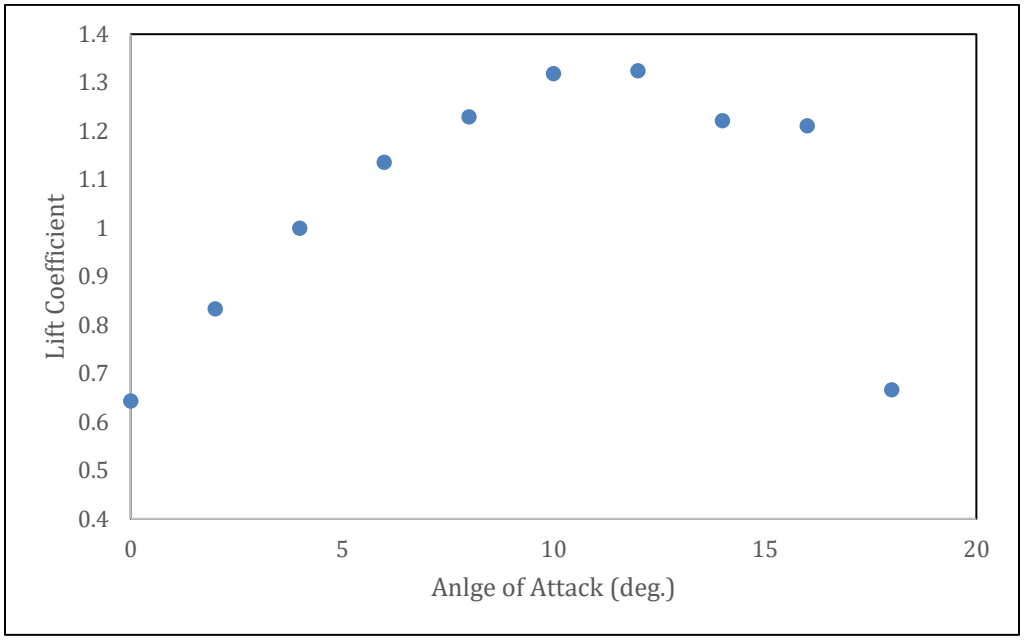

Figure 4: Boundary layer velocity distribution

Considerable research has been done with regards to boundary layer mitigation and subsequent improvement of airfoil lift characteristics. The physics behind such methods is simple yet effective. It is known that the fluid layer reverses direction when the kinetic energy diminishes due to viscous effects. If it were possible to somehow increase the kinetic energy of the fluid layer, it would be possible to delay boundary layer separation. A very common mitigation technique is the introduction of tiny devices known as vortex generators (VG) upstream of the separation point[4]. These devices induce swirl which moves higher momentum fluid into the lower momentum near wall region thereby increasing the turbulence of the flow. The fluid layer has more kinetic energy now to negotiate the adverse pressure gradient thus delaying the separation point. As a result, the wake region minimizes leading to larger lift coefficient values. In addition to vortex generators, there are other methods such as the use of synthetic jet actuators

to introduce vortices to enhance performance[5]. The VG was the chosen technique due to its simplicity.

A very detailed study on low profile vortex generator shape, size, and upstream placement and arrangement has been conducted by Lin[6]. These VGs had a maximum height of 50% of the boundary layer thickness and were placed just upstream of the separation point. The reader is encouraged to refer to Lin[6] for a more in-depth understanding of the various VG configurations. For this paper, vane type VG was considered. These VGs can be arranged in either a co-rotating or counter-rotating configuration; the latter was chosen for this study as seen in Fig. 5. For each configuration, factors such as stagger angle and spacing will influence the VG performance, however, this is beyond the scope of this project. The main goal here was to perform a basic research on mitigation techniques and demonstrate this effect numerically and experimentally.

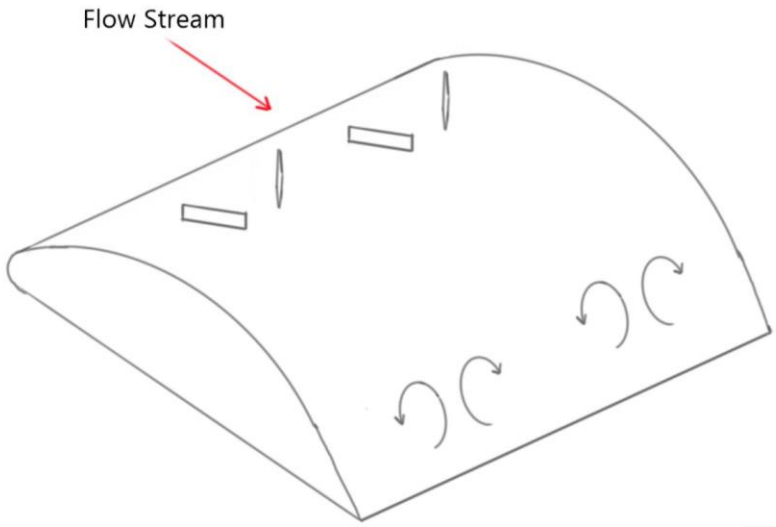

Figure 5: Counter rotating VG configuration

The present work is divided into numerical and experimental sections. First, the airfoil of interest, a NACA 4414, was selected. The airfoil coordinates were generated using an online airfoil generator (Airfoiltools) and imported into SolidWorks, a CAD software. For the numerical portion, the 2D airfoil was tested using ANSYS FLUENT, a Computational Fluid Dynamics (CFD) software, and the lift coefficient was computed at various angles of attack. The 3D model was then developed by adding a span to the airfoil and further numerical tests were done to validate results and identify the critical angle of attack. Following this, six different VG arrangements were tested at an angle of attack greater than the critical value. The arrangement that gave the maximum lift and minimum drag coefficients was selected. The experimental portion consisted of 3D printing the NACA 4414 airfoil, mounting pressure taps on the upper and lower surfaces, and testing the wing in the wind tunnel to obtain experimental values of lift coefficient with angle of attack. Subsequently, the VGs were then 3D printed and mounted onto the airfoil for further testing. The shape, size, placement, and arrangement of the VGs was consistent with that identified in the best case CFD trial. The project was an excellent learning experience where a problem was identified and a solution was developed using numerical and experimental techniques.

Methods

Numerical

The chosen airfoil was a NACA 4414 airfoil. The online airfoil generator, Airfoiltools, was utilized to create the profile as shown in Fig. 6. The maximum camber was 4.3% located at 40% chord length downstream of the leading edge. The maximum thickness was 14% while the number of points generated was 151. The airfoil coordinates were then imported to the CAD software, SolidWorks, to create the cross-section. The airfoil was given a chord length of 100 mm. Following this, the profile was imported into ANSYS Workbench 18.2 where the domain was created, meshed, and thereafter numerically analyzed in Fluent.

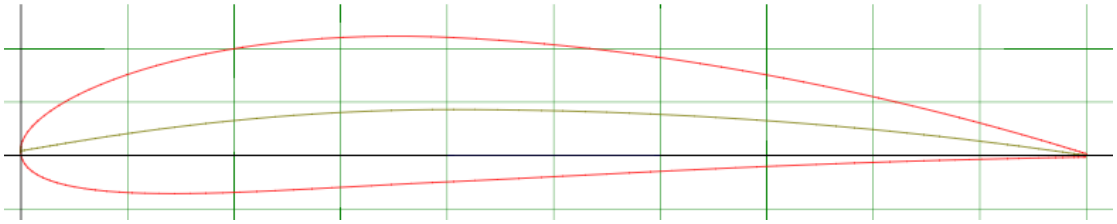

Figure 6: NACA 4414 airfoil from profile generator

Next, a basic grid independence study was carried out and the final mesh was selected. Three different levels (1, 2, and 3) of mesh were tested and the midlevel one was selected to save computational power. The difference in results between level 2 and level 3 mesh refinement was insignificant. Figure 7 shows the domain that was used. An inflation layer (see Fig. 8) at the airfoil surface was given so that the boundary layer behavior could be captured more accurately. For simplicity purposes, the domain chosen was a rectangular one, however, it is acknowledged that a more optimal mesh could have been achieved if time constraints were not present. The domain had a constant velocity inlet and a pressure outlet while the top and bottom were pressure far field. To ensure that the grid was apt and the CFD setup was correct, the Clark-Y airfoil was analyzed numerically using the same grid and setup parameters and the results were compared to experimental data from Lyon et al.[7] Both sets of data were at a Reynolds number of 200,000. The results were in close agreement thereby validating the numerical setup.

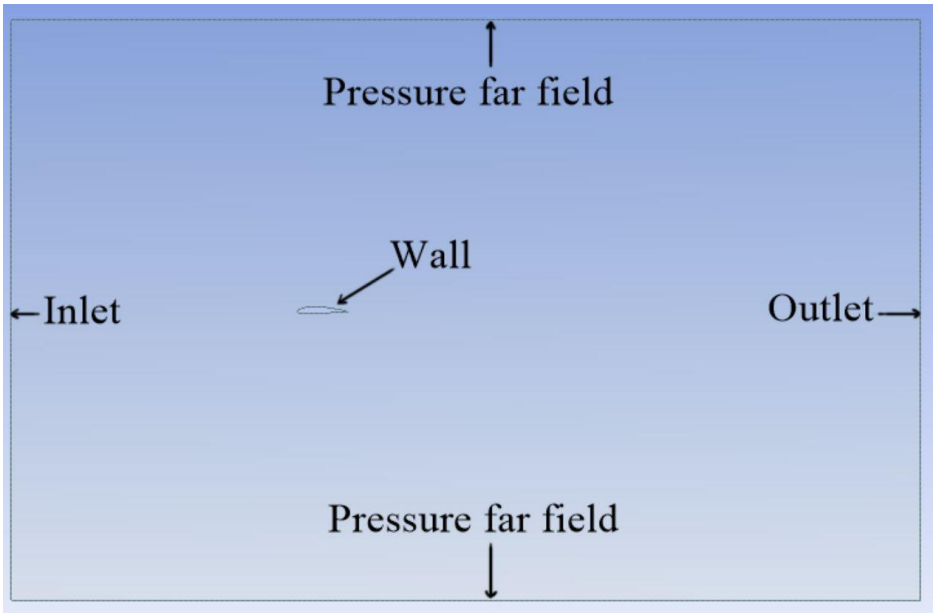

Figure 7: Domain labeled

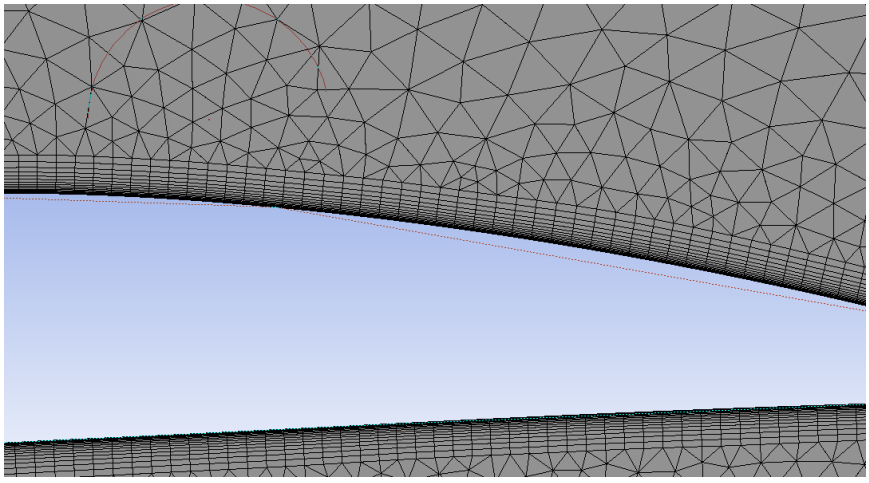

Figure 8: Zoomed in view of inflation layer

Table 1 below provides the various parameters and properties that were utilized in CFD.

Table 1: CFD Parameters

Chord Length	100 mm
Turbulence Model	Spalart-Allmaras
Momentum	Second Order Upwind
Pressure-Velocity Coupling	Simple
Inlet Velocity	30 m/s
Air Temperature	300 K
Air Density	1.225 Kg/m^3
Air Viscosity	$1.7894x10^{-5}$ Kg/(m-s)
Outlet Gauge Pressure	0 Pa
Wall	No slip

Since the vortex generators require a 3D analysis, the base NACA 4414 airfoil was extruded to a finite length in SolidWorks to create a wing as shown in Fig. 9. This was then imported into ANSYS Workbench, meshed, and analyzed in Fluent. The 3D wing demands much more computational power, therefore, two slices were created on either side of the wing center point so that only a portion (20 mm) of the wing needed to be analyzed (see Fig. 10). The two exposed surfaces were given a symmetric boundary condition. An inflation layer, just like for the 2D case, was also added.

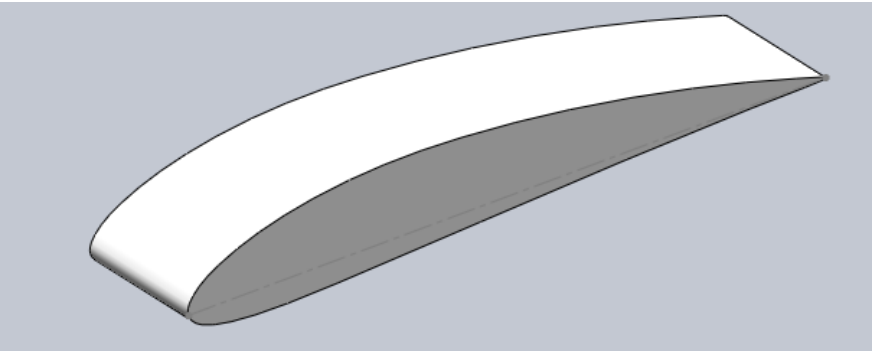

Figure 9: NACA 4414 3D wing

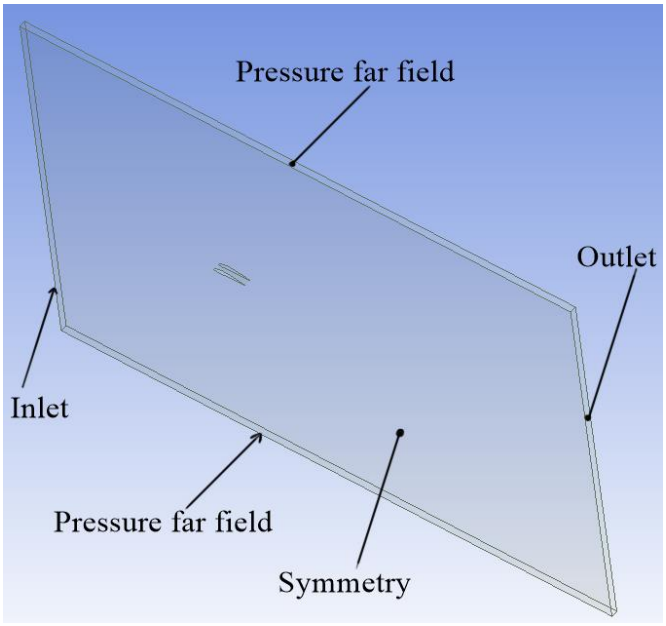

Figure 10: 3D NACA domain

The final part was the creation of the vortex generators. These were also created in SolidWorks after which they were assembled onto the wing. Figure 11 shows the vanes mounted onto the wing. Six different VG configurations were created, but only one of them is shown below for illustration purposes.

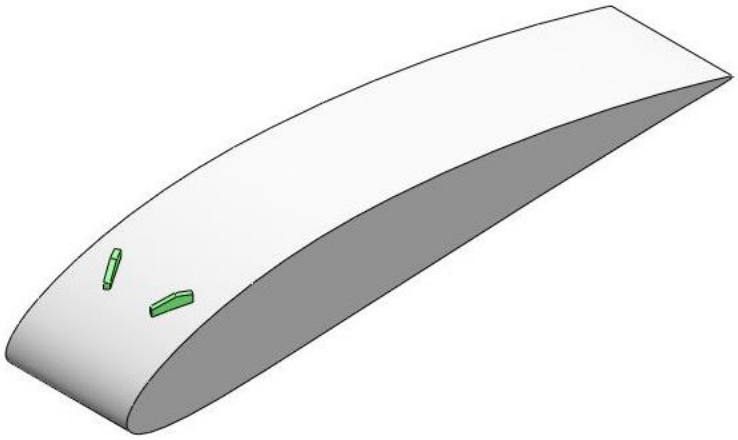
Figure 11: 3D NACA airfoil with VG mounted

Experimental

Following the generation of the NACA 4414 spatial coordinates, the airfoil was created in SolidWorks. The cross-section was then extruded to create a wing. The interior material was removed so that a hollow structure could be produced. This was required since pressure taps had to be mounted on the pressure and suction sides of the wing. Next, 1 mm diameter holes were created on both surfaces at Stagnation point (0%), 10%, 20%, 30%, 40%, 50%, 60%, and 70%

chord lengths. Additionally, an extra hold was created on the suction side at 80% chord length. It was not possible to do the same on the pressure side due to space constraints. SolidWorks was used to remove a portion of the bottom of the wing and turn it into a snap on cover to aid in assembly. This design was decided upon after several unsuccessful attempts to mount pressure taps on the original wing. The cover provided the accessibility required. Figure 12 is a CAD model of the finalized wing and the base cover ready to be 3D printed.

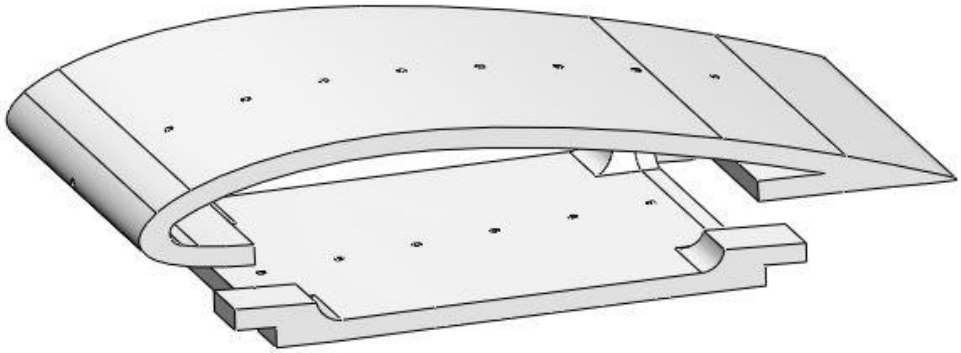

Figure 12: Image of CAD model of NACA 4414 middle section and cover

Both components were printed on a Dimension SST 1200es 3D printer. A 100% infill with a layer height of 0.006 in. was chosen in order to produce accurate yet sturdy components. The printing orientation of each component was carefully chosen to ensure that the polymer layers were aligned parallel to the direction of fluid flow so that adverse effects due to surface roughness were minimized. The printing material chosen was Acrylonitrile Butadiene Styrene P430 (ABS-P430). The platform and all support structures were made up of soluble P400SR material. Once the components were printed, they were placed in a CleanStation reservoir filled with a mixture of water and P400SC concentrate to dissolve the supporting structures. Depending on the size of the component, this process lasted anywhere from one to eight hours. Surface imperfections, as a result of the print, were smoothed out using a 220 grit sandpaper after which the airfoil was washed with soap and water. The biggest challenge during 3D printing was the presence of warpage. The middle portion of the airfoil was printed numerous times with various methods to try to reduce the likelihood of warping. This is an area that is currently being researched very extensively by many. Initially, the component was printed out of a Nylon resin, this proved to be more susceptible to warping, for this reason, ABS was decided upon.

The most critical assembly operation was mounting of the pressure taps on the airfoil. This was completed by using a 1.59 mm drill bit to increase the diameter of the holes which were printed into the middle section of the airfoil. Following the drilling, the pre-cut pressure taps were then press fitted into the airfoil's 2.54 mm thick walls mechanically. The pressure taps measured 1.65 mm outer diameter, 1.35 mm inner diameter, and 4.06 mm in length. Since the holes were already printed normally to the airfoil surface, the mounting orientation was relatively easy. Masterflex Tygon tubing with an inner diameter of 1.52 mm was used to connect the taps to the manometer bank. SureHold Plastic Surgery glue was used to secure the taps in place. With this, the mid-section of the wing was complete. Since the wing had to span the height of the wind

tunnel test section (300 mm or 12 inches) to ensure that side vortices were minimized, two separate spacers were 3D printed and affixed on to the mid portion using threaded rods shown in Figure 13. The tubing was then carefully run through the bottom spacer and the back cover was snapped on.

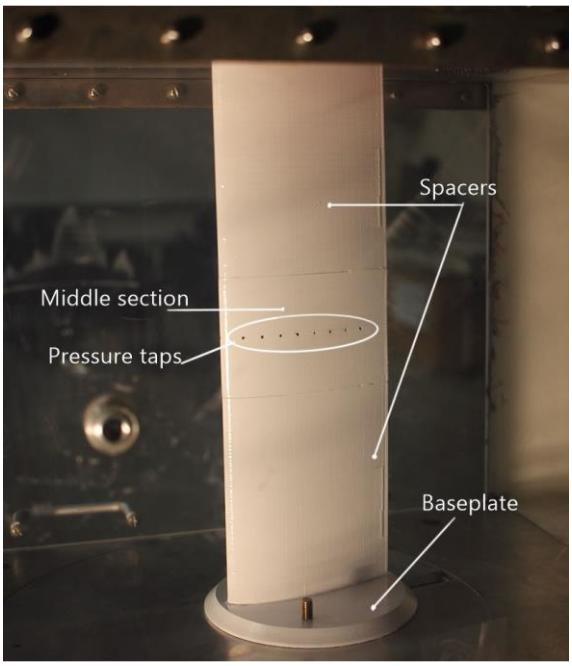

Figure 13: NACA 4414 final 3D printed airfoil

During the initial assembly phase, a major setback was encountered. The snap on cover at the bottom created weak points and as a result, the original cover fractured due to the large amount of tubing inside the airfoil impinging on it. The fractured cover is shown in Fig. 14. A new cover was manufactured and the tubes were repositioned carefully to minimize impingement.

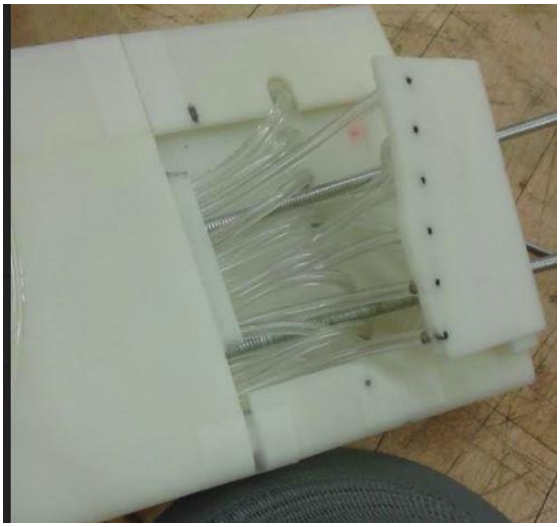
Figure 14: Fractured cover

Another challenge that had to be successfully navigated involved the last pressure port on the pressure side (70% chord length) of the airfoil. The interior spacing available to mount the Tygon tube was very minimal such that special care had to be taken. A portion of the aft of the airfoil was milled using a Bridgeport manual milling machine as shown below. Once this was done, it was relatively easier to connect the tube.

Figure 15: Utilizing a manual milling machine to remove material necessary to fit Tygon tubing

Once experimental testing of the base wing was complete, the vortex generators had to be manufactured and mounted so that additional testing could be conducted to study the new flow behavior. First, the VG dimensions had to be determined. According to Lin[6], the maximum height was 50% of the boundary layer thickness. For the current experiment, this meant that the VG height needed to be around 0.05 mm. A single layer of 3D printed material is itself around 0.05 mm and due to this tolerance constraint, the minimum stable height that could be printed was 1.5 mm. The VG was printed to this size and carefully sanded down to 1.15 mm which was roughly the height of the selected VG from numerical analysis. Figure 16 below shows a zoomed in view of the printed VGs mounted onto the airfoil. In order to ensure that each VG was in the correct location, a template was created and affixed to the airfoil which showed the proper location of each VG. The positions were marked, the template was removed and the VGs were affixed. A double sided tape was used to affix the VG onto the airfoil suction side.

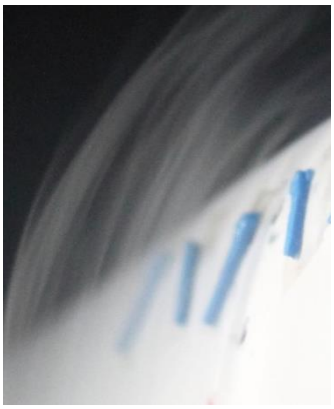

Figure 16: The VGs mounted on to the airfoil

Results and Discussion

Numerical Results

The first set of results to be analyzed were those from the 2D trials of the Clark-Y airfoil (Re = 200,000) for validation purposes. Figure 17 shows the close agreement thus validating the CFD model.

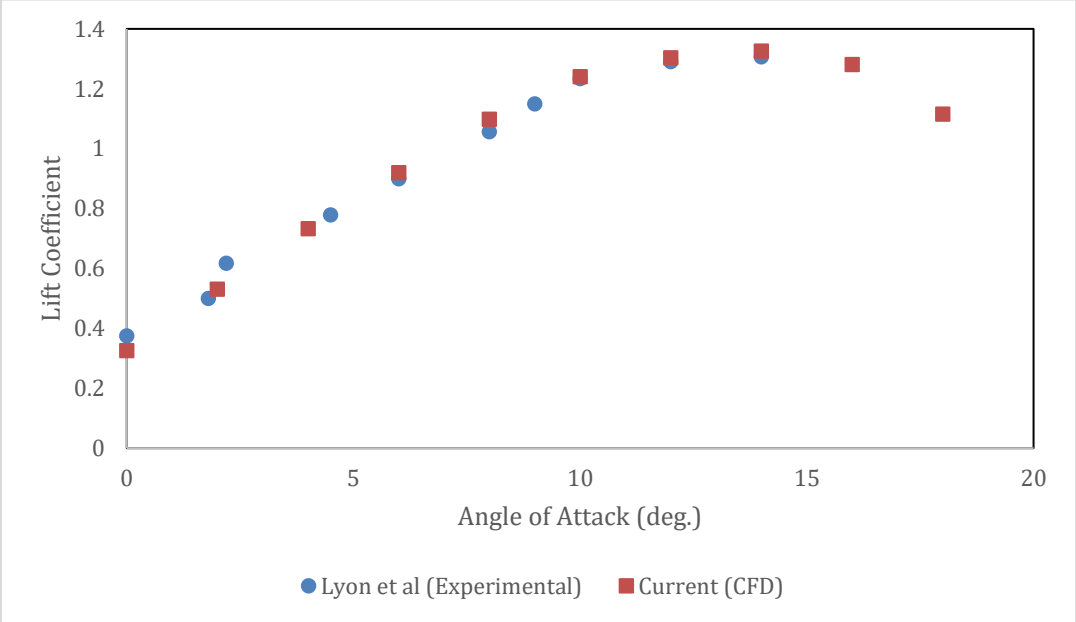

Figure 17: Comparison of published and CFD values of lift coefficient

Once the numerical setup was established, the NACA 2D was then analyzed and the results of lift coefficient at various angles of attack were documented as seen in Fig. 18. The procedure was repeated for the 3D wing. Both results were in close agreement, therefore, only a few data points for the 3D case are shown below.

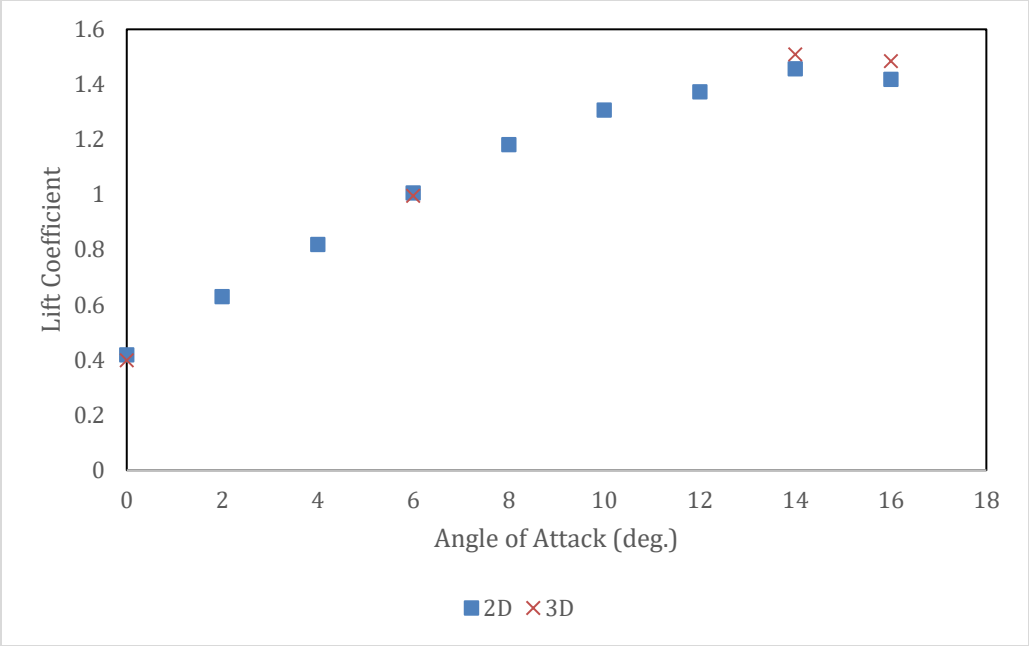

Figure 18: NACA 4414 lift coefficient vs. angle of attack for 2D and 3D CFD runs

The critical angle of attack was noted to be 14 deg. Since stalling is our main point of interest, the figures below illustrate the velocity and pressure contours and a zoomed in view at the boundary layer at 16 deg. angle of attack when the wing has stalled.

Figure 19 is a velocity contour plot. As expected, the flow speeds up at the tip of the airfoil thus resulting in a lower pressure on the upper surface as seen in Fig. 22. Additionally, it can be seen that the wing has stalled since there is a large wake at the trailing edge.

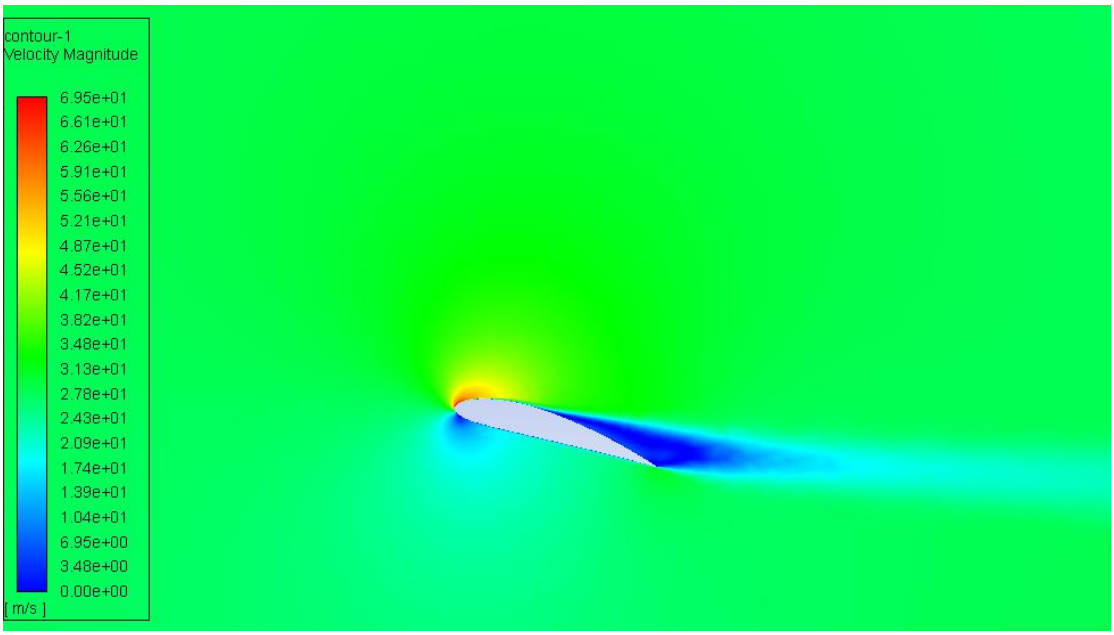

Figure 19: NACA 4414 Velocity contour at 16 deg.

To confirm the theory, the fluid layer near the airfoil was examined by looking at the vector profile as shown below. The vectors were tracked along the airfoil suction side and the point at which the first vector reversed was noted; this occurred at 43.5% of chord length from leading edge. The series of pictures in Fig. 20 show the velocity profile clearly and it matches with what was learned in theory. Figure 21 shows the reversed vectors veer off from airfoil and form vortices going downstream.

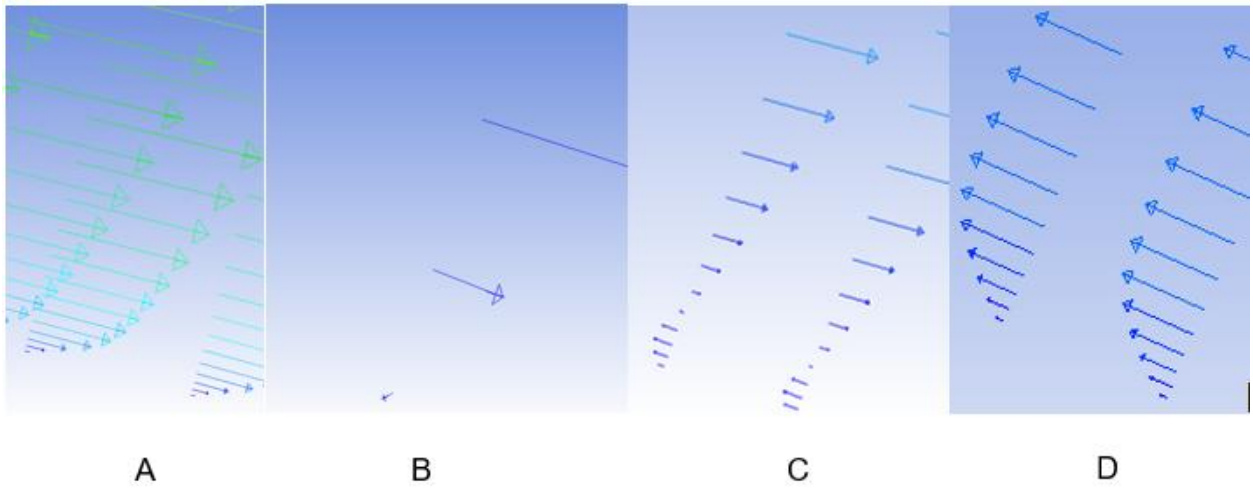

Figure 20: Velocity vector profile A) Upstream of first reversal point B) First point of flow reversal C) Downstream of reversal point D) Complete flow reversal in wake region

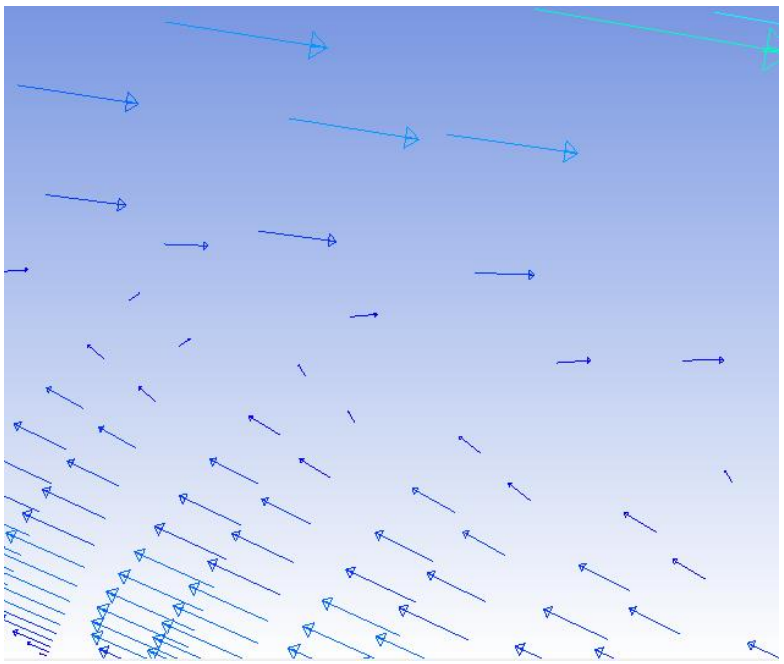

Figure 21: Flow leaving the airfoil and forming circulation zone

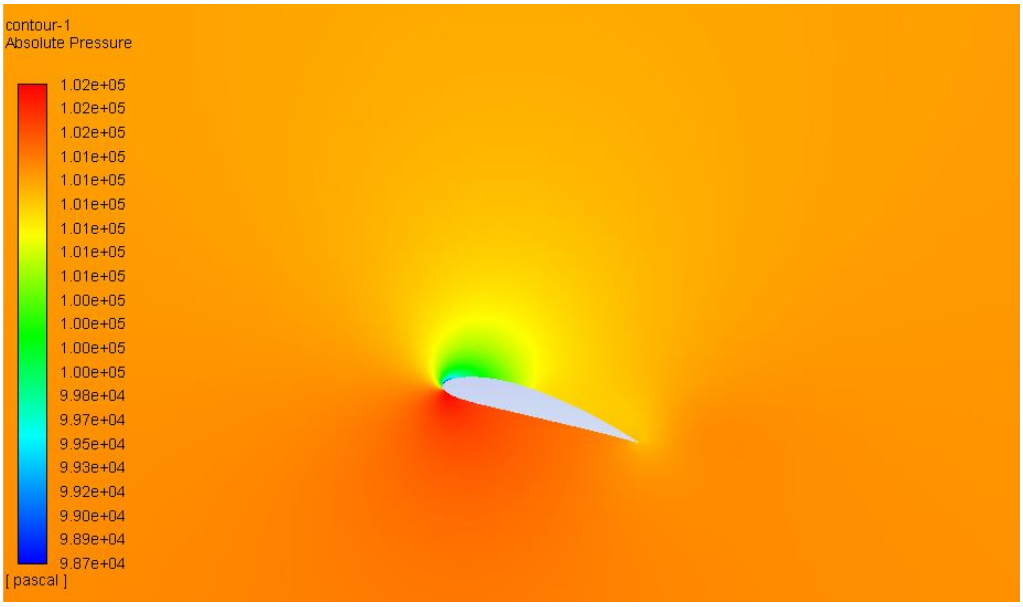

Figure 22: Absolute pressure contour of NACA 4414 at 16 deg.

Stalling, as mentioned in the introduction, is highly undesirable and to mitigate this phenomenon, vortex generators were to be mounted onto the wing and analyzed. Six different VG configurations were looked into and each configuration was numerically analyzed at an angle of attack of 18 deg. The arrangement that gave the highest lift coefficient and lowest drag coefficient compared to the base airfoil case was selected for further CFD and experimental analysis. Figure 23 below highlights the important parameters tested while Table 2 lists the results and Fig. 24 gives an isometric view of all vane configurations analyzed. The parameters of interest were incidence angle (β), height (H), length (L), and normalized chord location from leading edge.

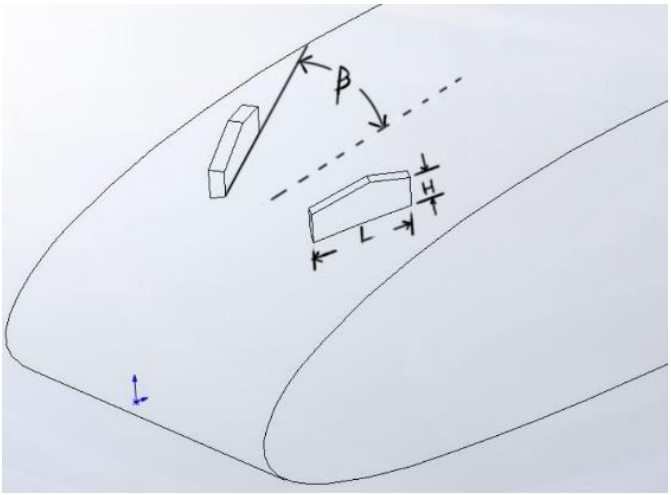

Figure 23: Sample VG arrangement.

Table 2: Various tested VG configurations with respective lift and drag performances

VG Configuration	Height (mm)	Length (mm)	Location Along Chord	Angle of Incidence	Increase in Lift (%)	Decrease in Drag (%)
1	0.76	4	15%	20	4.73	0.05
2	1.76	4	15%	20	-10.41	-25.16
3	1.6	5	15%	20	-5.39	-14.58
4	1.51	5	10.50%	20	24.52	8.58
5	1.01	5	10.50%	20	25.14	11.08
6	1.14	5	10.50%	30	26.43	17.23

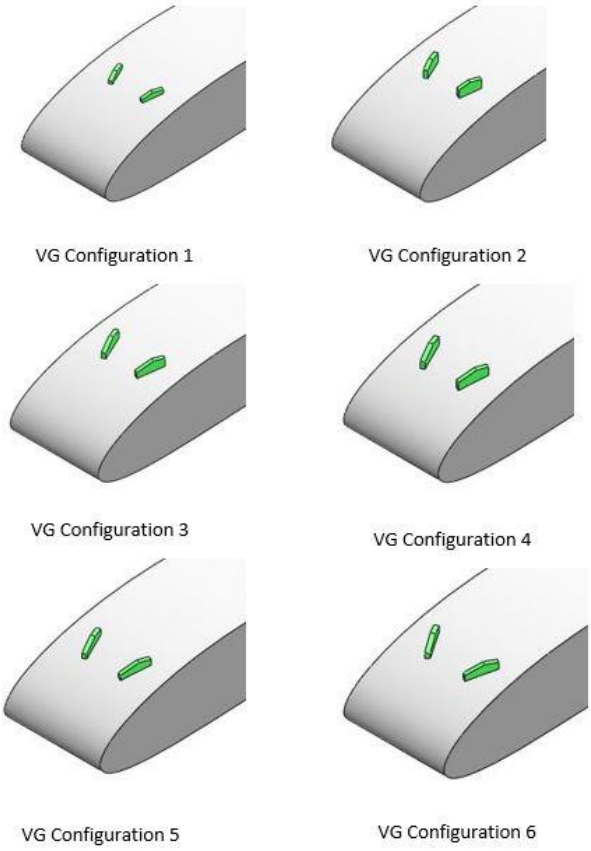

Figure 24. Isometric view of all VG configurations tested

It is evident from Table 2 that configuration 6 provided the best results. The following images pertain to this particular arrangement. The images have been taken at the center plane of the airfoil, i.e. plane bisecting the middle of the 2 VGs and thus the VGs are not visible. For convenience purposes, Fig. 25 shows a side view of this configuration. Figure 26 is the velocity contour plot while Fig. 27 is the corresponding pressure plot.

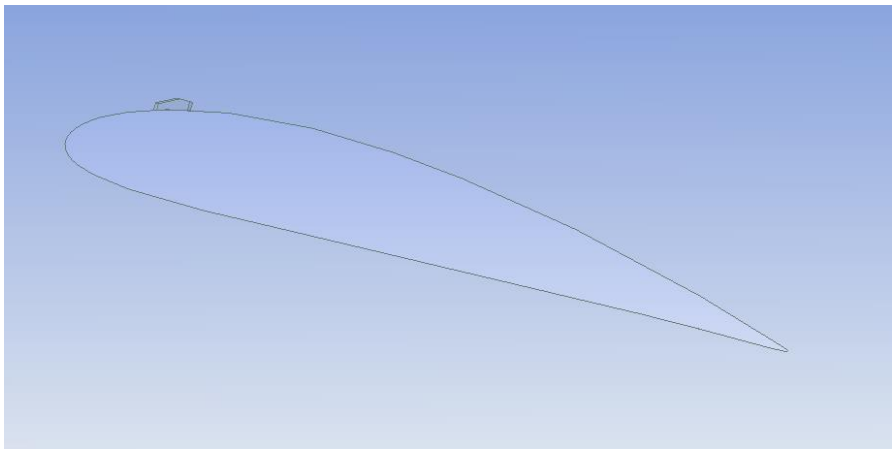

Figure 25: Side view of chosen configuration with VG mounted

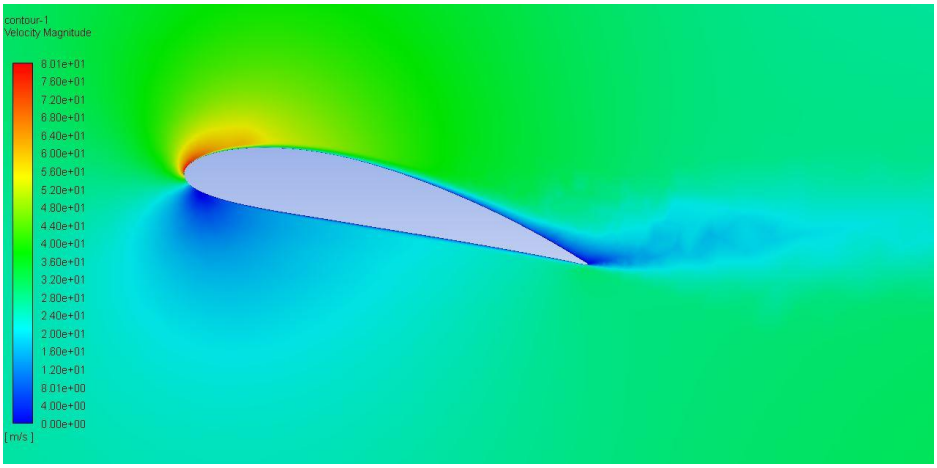

Figure 26: Velocity contour

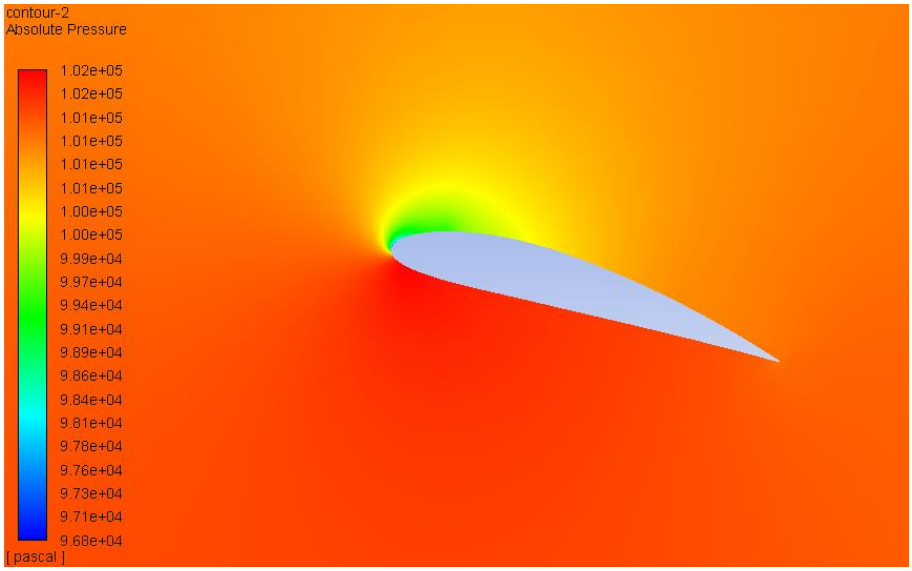

Figure 27: Pressure contour

From comparing Figs. 26 and 19, and Figs. 22 and 27, it is clear that the VG has dramatically improved the flow. The wake region has shrunk and moved almost to the trailing edge. Tracking the velocity vectors in the boundary layer showed that the first vector reversal happened at 97% chord length from leading edge as opposed to 43.5% for the base case. This improvement is remarkable and can be seen in the lift coefficient vs. angle of attack graph below. Initially, the VG does not aid in lift and this is expected according to the literature. However, at higher angles of attack, the difference in performance is visible. In fact, the stall angle occurs now at 16 deg. as opposed to 14 deg. This confirms that vortex generators in the correct arrangement will improve airfoil performance.

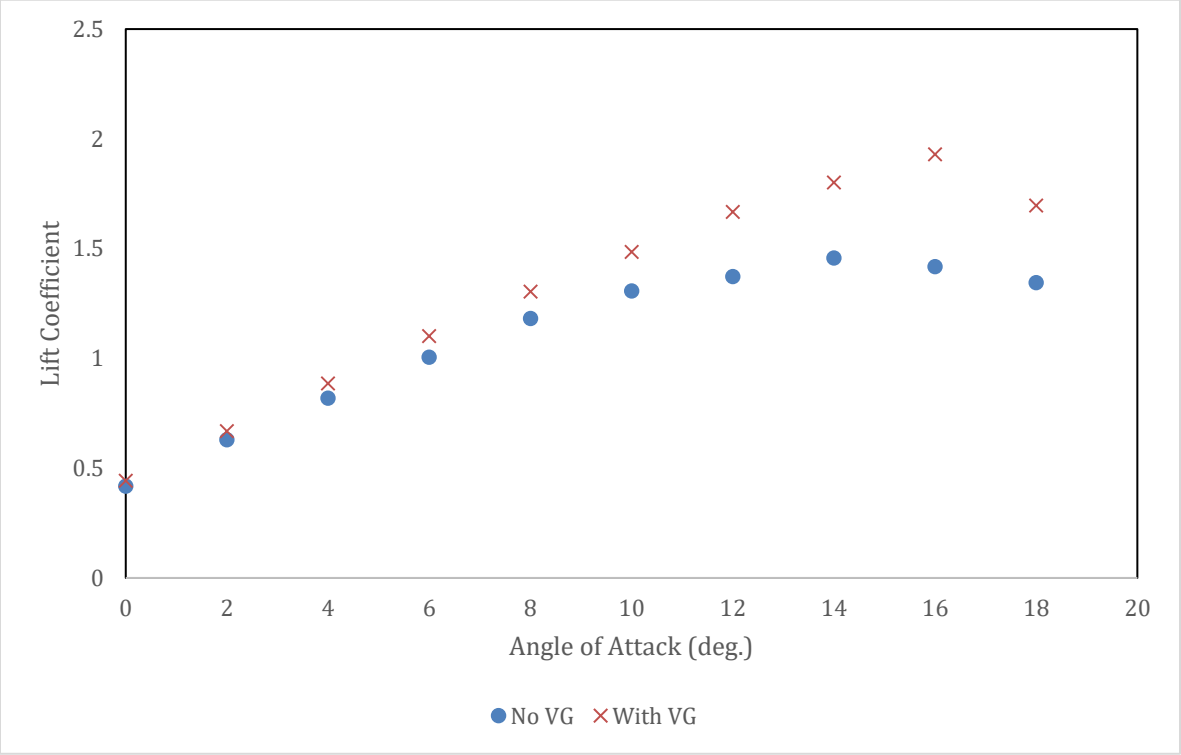

Figure 28: CFD comparison of lift coefficient with angle of attack for wing with and without VG

The numerical study facilitated the study of various VG configurations and allowed the authors to select the right configuration without trial and error thereby saving enormous amounts of time. The next section highlights the experimental results.

Experimental Results

Once the completed wing was mounted in the Aerolab wind tunnel, the tubes were then connected to an Aerolab manometer bank and the fan was started. A manometer was mounted at the entrance of the test section so that the air speed could be determined. A water height of 2.2 inches was maintained for all experiments; this corresponds to 30 m/s airspeed. Figure 29 shows this setup. The angle of attack was then adjusted manually using the baseplate of the wind tunnel which had already been calibrated. Following the base case runs, the selected VG configuration 6

was mounted onto the wing and tests were conducted. The results are given in Fig. 30 (see appendix for lift coefficient determination).

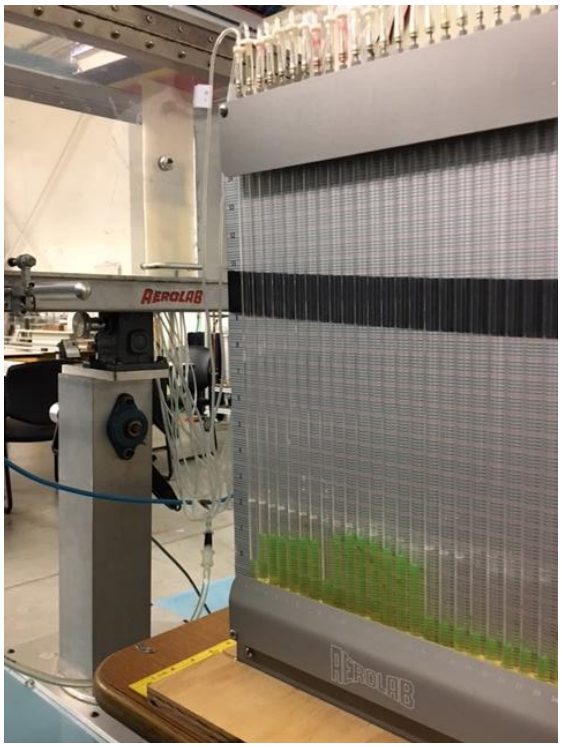

Figure 29: Airfoil mounted in wind tunnel and connected to manometer bank

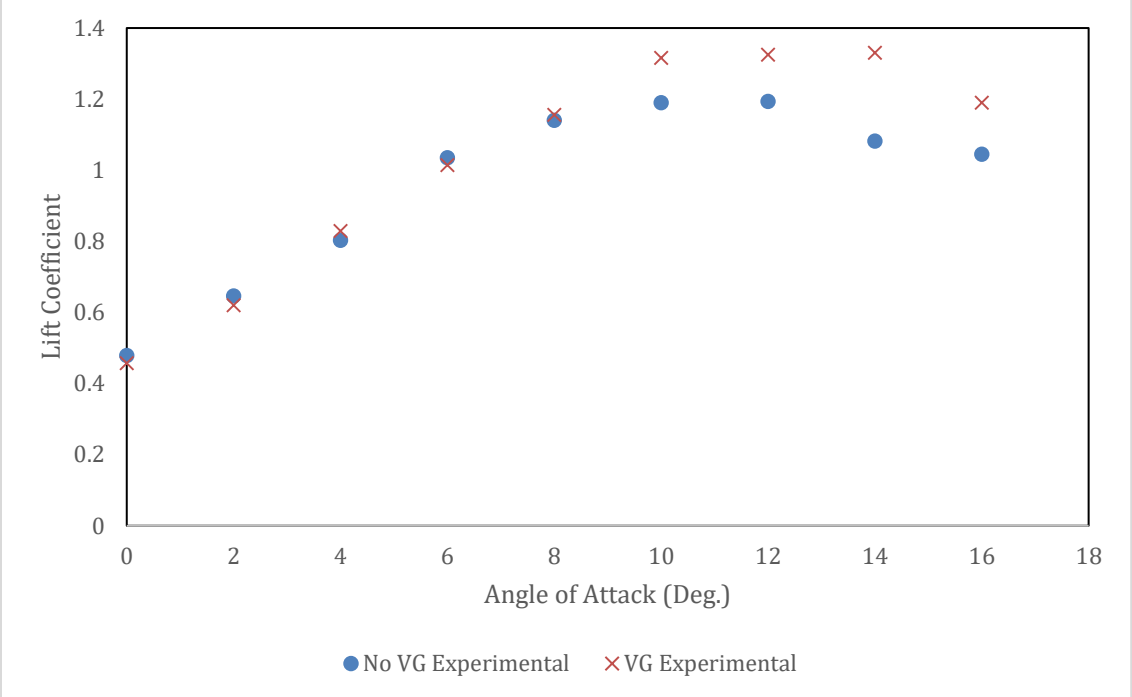

Figure 30: Experimental values of lift coefficient with angle of attack for NACA 4414 wing with and without VG

Figure 30 confirms what was established in the numerical study. The VG does not affect the lift coefficient initially, but at higher angles of attack, the effect is visible. The base wing stalls at 12 deg. but with the VG added on, the stall is delayed until 14 deg. This was consistently different by 2 deg. from what CFD predicted. Several factors could be responsible for the difference between the numerical and experimental results. For starters, the CFD simulation assumed a smooth wing and VG surface. This was clearly not the case for the wing and VG manufactured. Errors could have also been introduced when reading the water height values from the rake and subsequent coefficient of pressure calculations. However, the main point to note is that the results from both methods had similar trends. The CFD and experimental comparison for the base wing and with VG is given below.

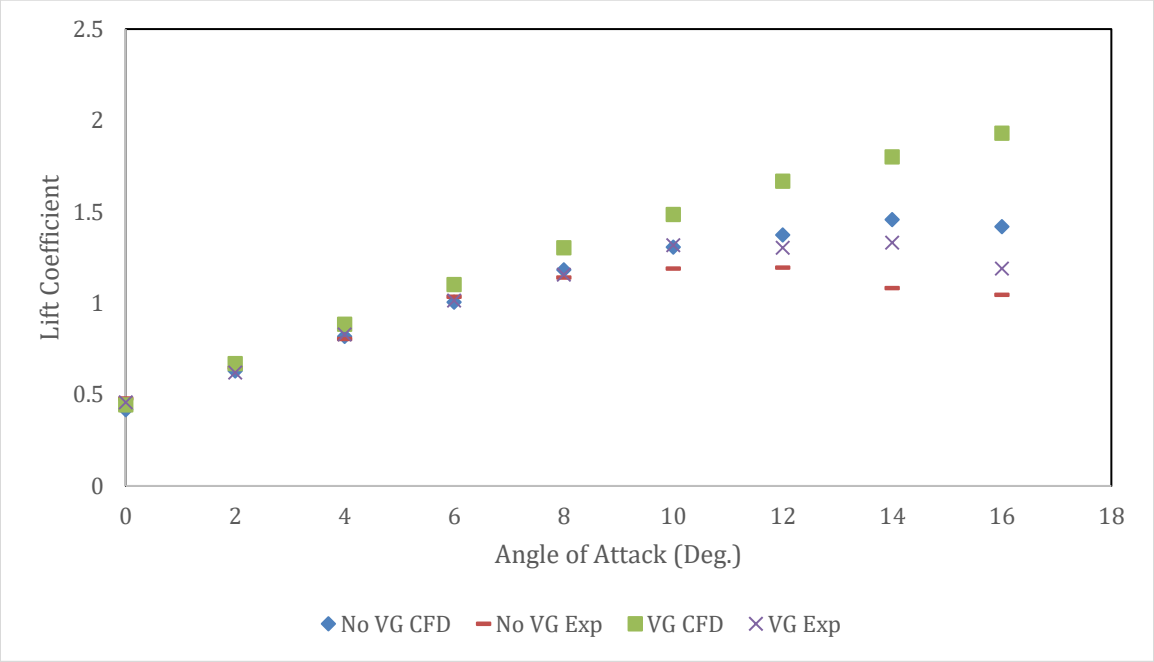

Figure 31: NACA 4414 wing CFD and experimental data comparison

Conclusions

A numerical and experimental analysis was conducted for a custom NACA 4414 airfoil. The numerical simulation was verified with published data for a Clark-Y airfoil. Following this, a 2D and 3D study on the NACA airfoil was done and lift coefficient with various angles of attack documented. The wake region was noticed and flow behavior in the boundary layer was observed. Six different vortex generator (VG) configurations were then tested and the best one selected. Further analysis was conducted and it was observed that the lift performance increased drastically due to the fact that the boundary layer separation point was pushed almost to the wing end point. Experiments were then conducted for the wing with and without VG mounted. The results aligned very well with what was predicted numerically. The project provided a medium for an all rounded study on a certain topic of interest.

Bibliography

[1] Munson, Bruce, Donald Young, and Theodore Okiishi, *Fundamentals of Fluid Mechanics*, Wiley, 5th ed., 2006.

[2] Pritchard, Philip, Mitchell John, and John Leylegian, *Introduction to Fluid Mechanics*, Wiley, 9th ed., 2015.

[3] Cengel, Yunus and John Cimbala, *Fluid Mechanics Fundamentals and Applications*, McGraw Hill, 1st ed., 2006.

[4] Aider, J., Beaudoin, J., Wesfreid, J., *Drag and Lift Reduction of a 3D Bluff-Body Using Active Vortex Generators*, *Experiments in Fluids*, 2010, Vol. 48 (5), pp. 771-789.

[5] Chaudhry, I, A., Sultan, T., Siddiqui, F, A., Farhan, M., Asim, M., *The Flow Separation Delay in the Boundary Layer by Induced Vortices*, *Journal of Visualization*, 2016, Vol. 20 (2), pp. 251 – 261.

[6] Lin, J. C., *Review of Research on Low-Profile Vortex Generators to Control Boundary-Layer Separation*, *Progress in Aerospace Sciences*, 2002, Vol. 38, pp. 389 – 420.

[7] Lyon, A. Christopher, Andy P. Broeren, Philippe Giguere, Ashok Gopalarathnam , and Michael S. Selig, *Summary of Low-Speed Airfoil Data*, SoarTech Publications, Volume 3, 1997.

Appendix

Lift coefficient computation

Once the manometer bank water levels were read, they were converted to pressure values and the coefficient of pressure (C_P) was determined from the following equation.

$$C_p = \frac{P - P_\infty}{0.5 * \rho * V_\infty^2}$$

Where: P is the static pressure, P_∞ the freestream static pressure, ρ the density of air, and V_∞ the freestream velocity.

The lift coefficient C_L was then computed from the pressure coefficient as follows:

$$C_L = cos\alpha \int_0^1 C_P \, d\eta$$

Where: η= normalized chord length

The above integral involved evaluating the area under a graph of pressure coefficient vs. normalized chord length. A typical graph of C_P vs. η is shown below. A MATLAB code was written so that the area enclosed by the curve could be computed.

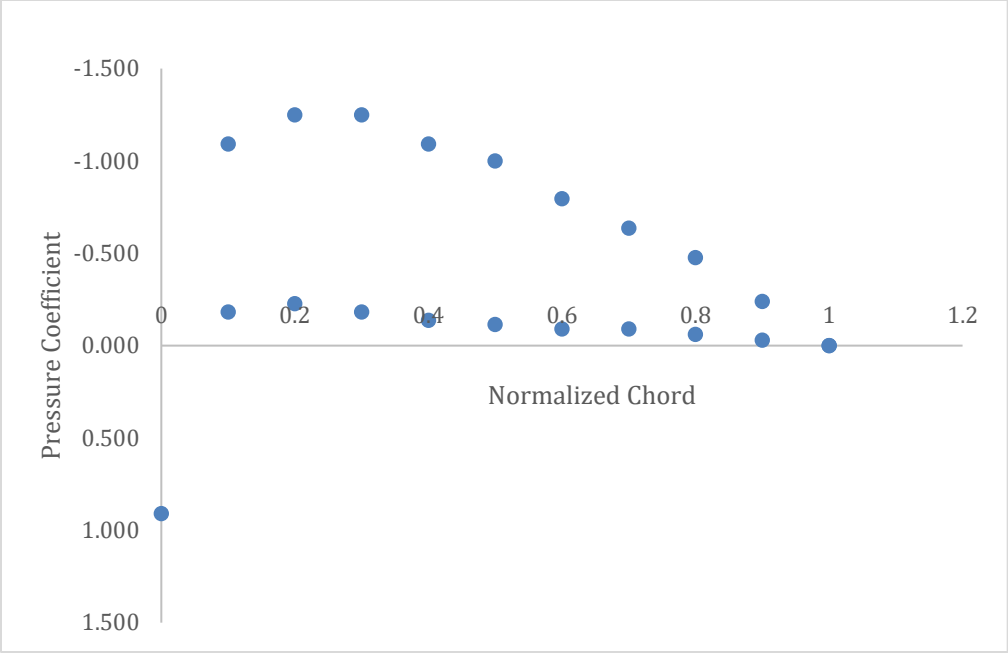

Figure A1: Pressure coefficient vs. normalized chord length for a NACA 4414 airfoil trial